Journal of Molecular Catalysis A: Chemical 304 (2009) 88–94

Contents lists available at ScienceDirect

Journal of Molecular Catalysis A: Chemical

journal homepage: www.elsevier.com/locate/molcata

Chirality inversion in enantioselective hydrogenation of isophorone over Pd/MgO catalysts in the presence of (*S*)-proline: Effect of Pd particle size

Shuang Li[a], Chunhui Chen[a], Ensheng Zhan[a], Shang-Bin Liu[b,*], Wenjie Shen[a,**]

[a] *State Key Laboratory of Catalysis, Dalian Institute of Chemical Physics, Chinese Academy of Sciences, Dalian 116023, China*
[b] *Institute of Atomic and Molecular Sciences, Academia Sinica, Taipei 10617, Taiwan*

ARTICLE INFO

Article history:
Received 7 August 2008
Received in revised form 19 January 2009
Accepted 20 January 2009
Available online 30 January 2009

Keywords:
Chirality inversion
Isophorone
3,3,5-Trimethylcyclohexanone (TMCH)
(*S*)-Proline
Enantioselective hydrogenation
Kinetic resolution

ABSTRACT

Enantioselective hydrogenation of isophorone in the presence of (*S*)-proline was examined over a series of Pd/MgO catalysts with varying Pd particle size. It was found that the Pd surfaces not only supply chemisorbed hydrogen required for the hydrogenation of isophorone but also be involve in the enantio-differentiating step. Moreover, it was observed for the first time that the configuration of the chiral product could be tuned by varying the size of Pd particle such that (*R*)-TMCH rather than (*S*)-TMCH was obtained over the Pd/MgO catalysts with large Pd particles. Two competitive reaction pathways during the enantioselective hydrogenation of isophorone were proposed depending on the size of Pd particle. One involves the enantioselective hydrogenation of the reaction intermediates formed on large Pd particle with size exceeding 10 nm leading to the excess formation of (*R*)-TMCH enantiomer, whereas the other invokes the primary hydrogenation of isophorone to racemic TMCH over Pd particle with size smaller than 4 nm, followed by the kinetic resolution process leaving the (*S*)-TMCH enantiomer in excess.

1. Introduction

In view of the rapidly increasing interest in practical applications, heterogeneous enantioselective hydrogenations over supported metal catalysts in the presence of chiral modifiers have been extensively studied. Among them, the enantioselective hydrogenations of α-ketoesters over Pt/cinchona [1] and β-ketoesters over Raney Ni/tartaric acid [2] are the well-established processes [3]. It is generally recognized that the enantioselectivity during the hydrogenation of these ketones is provoked by the chiral center, which is introduced by the chiral modifier, and that the enantio-differentiation step takes place predominately on the modified metal surfaces [4–6]. However, the equally important enantioselective hydrogenation of the C=C bond has received much smaller attention than it deserves [7–9]. The representative example is the enantioselective hydrogenation of isophorone over Pd catalysts in the presence of (*S*)-proline to (*S*)-3,3,5-trimethylcyclohexanone (TMCH). Tungler et al. [10–12] initially reported a moderate enantioselectivity of about 60% over Pd/C catalysts. However, the stoichiometric amount of (*S*)-proline is normally believed to act only as a chiral auxiliary because its presence does not multiply the chirality [6,7,11–14]. (*S*)-proline is initially condensed with isophorone to form the reaction intermediates, which are further hydrogenated to generate the enantioselectivity. Hydrogenation of the C=C bond of the reaction intermediates would produce (*S*)-TMCH, while further hydrogenation of the intermediates would form undesired by-products.

Török and co-workers [15,16] further improved the e.e. value as high as 99% by using Pd catalysts supported on solid bases, such as alkaline earth metal carbonates. They concluded that the key step is the adsorption of (*S*)-proline on the support and that the secondary kinetic resolution of TMCH occurs on the surface linked proline [16]. Quite recently, they further proposed a unified mechanism with additional experimental evidence, in which the secondary kinetic resolution is mainly responsible for high enantioselectivity, strongly depending on the catalyst [17].

On the other hand, Lambert et al. [18,19] have recently reported that the enantioselectivity in the hydrogenation of isophorone is merely the result of a kinetic resolution process which occurs homogeneously in the solution and that the metal surface does not play a role in the enantio-differentiating step. As such, racemic TMCH is produced during the rapidly occurring hydrogenation of isophorone at the initial stage, (*S*)-proline then reacts homogeneously and preferentially with the (*R*)-TMCH enantiomer, leaving the (*S*)-TMCH enantiomer in excess. In other words, the Pd particle only catalyzes the hydrogenation of isophorone to racemic TMCH and is not involved in the enantio-differentiation step. Hence, the nature of the enantioselectivity and the reaction mechanism invoked during the hydrogenation of isophorone over Pd catalysts

* Corresponding author. Tel.: +886 2 23668230; fax: +886 2 23620200.
** Corresponding author. Tel.: +86 411 84379085; fax: +86 411 84694447.
E-mail addresses: sbliu@sinica.edu.tw (S.-B. Liu), shen98@dicp.ac.cn (W. Shen).

1381-1169/$ – see front matter © 2009 Elsevier B.V. All rights reserved.
doi:10.1016/j.molcata.2009.01.029

in the presence of (*S*)-proline still remain as controversial debates and challenging issues.

Our recent reports revealed that both the acid/base feature of the support and the size of Pd particle influenced the enantioselectivity during the hydrogenation of isophorone [20,21]. In particular, the Pd/MgO catalyst with enhanced proline adsorption and moderate Pd particle size was found to have a rather high enantioselectivity (e.g. 95%) with a modest TMCH yield (43%). As a continuation of our previous studies, the present work aims to investigate the effect of Pd particle size on the enantioselectivity during the hydrogenation of isophorone over Pd/MgO catalysts in the presence of (*S*)-proline.

2. Experimental

2.1. Preparation of the Pd/MgO catalysts

A commercially available MgO with a specific surface area of 24 m^2/g was calcined at 900 °C in air for 5 h before use, resulting in a notable decrease in surface area to 5 m^2/g. The Pd/MgO catalysts were then prepared by using the impregnation method: 0.842 g of $Pd(OAc)_2$ was dissolved in 400 mL of acetone, and then mixed with 20 g of MgO (with a nominal Pd content of 2 wt%). The suspension was kept at 30 °C for 24 h under stirring and the mixture was vaporized in a rotary evaporator to remove acetone. The obtained yellowish powders were then subjected to calcination in air at 200–800 °C for 5 h. These samples are hereafter denoted as PdO/MgO-T_1, where T_1 represents the temperature of calcination. The PdO/MgO-T_1 samples were further reduced by hydrogen at a desirable temperature, which varied from 200 to 600 °C. These catalysts are denoted as Pd/MgO-T_1–T_2, where T_2 refers to the temperature of hydrogen reduction.

2.2. Catalyst characterization

The actual loading of Pd in the catalyst was estimated to be 1.49 wt% by inductively coupled plasma atomic emission spectroscopy (ICP-AES), using a Leaman Plasma-Spec-I spectrometer.

Transmission electron microscopy (TEM) images were taken on a Philips Tecnai G^2 Spirit instrument operated at 120 kV. Each specimen was prepared by suspending the catalyst sample in ethanol under ultrasonication. Droplets of the suspension were then applied onto a clean carbon-enhanced copper grid and dried in air.

Powder X-ray diffraction (XRD) patterns were recorded on a D/Max-2500/PC Diffractometer (Rigaku, Japan) using nickel-filtered Cu Kα radiation operated at 40 kV and 100 mA. The crystalline sizes of Pd and MgO were calculated by using the Scherrer equation [22].

Chemisorption of CO was conducted using an Auto Chem 2910 instrument (Micromeritics, USA) at 40 °C. Prior to the measurement, the sample was treated in He at 400 °C for 2 h, followed by reduction with hydrogen at 200 °C for 1 h.

Temperature-programmed reduction (TPR) experiment was also conducted on the Auto Chem 2910 instrument equipped with a thermal conductivity detector (TCD). 100 mg sample was heated to 400 °C under Ar flow (50 mL/min). After cooled to −70 °C, the sample was exposed to a 5% H_2/Ar mixture (50 mL/min), and then heated to 800 °C at a rate of 10 °C/min.

Temperature programmed desorption (TPD) of CO_2 was performed on the same apparatus. 100 mg sample was treated in He at 400 °C for 2 h to remove the adsorbed impurities. After cooled to 40 °C in He, the sample was exposed to a 10%CO_2/He mixture for 30 min, followed by purging with He for 30 min, and then heated to 450 °C at a rate of 10 °C/min under He flow.

2.3. Hydrogenation of isophorone and kinetic resolution of TMCH

Hydrogenation of isophorone and kinetic resolution of TMCH were conducted in a stainless steel autoclave with a quartz liner at 40 °C and a hydrogen pressure of 3.0 MPa. The typical reaction system includes 32 mg catalyst, 110 mg (*S*)-proline, 1.18 mmol isophorone (or TMCH), and 8.8 mL ethanol as solvent, pre-mixed in a quartz tube. The tube was placed into a 50 mL stainless steel autoclave with magnetic stirrer. Prior to the reaction, the reaction mixture was initially stirred for 40 min and flushed with hydrogen three times. The products were analyzed by using gas chromatograph (Agilent 6890N) equipped with a β-cyclodextrin capillary column (Chirasil-Dex CB, Varian) at 110 °C and a flame ionization detector. To ensure the reliability of the determination of the amounts of isophorone and/or TMCH, n-octane was used as an internal standard. The conversion of isophorone and the yield of TMCH were calculated according to the following equations:

$$\text{isophorone conversion, \%} = 100 \times [\text{isophorone}_{\text{initial}} - \text{isophorone}_{\text{final}}]/[\text{isophorone}_{\text{initial}}]$$

$$\text{TMCH yield, \%} = 100 \times [\text{R} + \text{S}]/[\text{isophorone}_{\text{initial}}] \text{ for the hydrogenation of isophorone, and } = 100 \times [\text{R} + \text{S}]/[\text{TMCH}_{\text{initial}}] \text{ for the kinetic resolution of TMCH.}$$

3. Results and discussion

3.1. Physical and chemical properties of the Pd/MgO catalysts

Fig. 1 shows the TEM images of the PdO/MgO-T_1 samples. It is clear that the PdO particles are uniformly dispersed on the large MgO support. With increasing calcination temperature, a notable increase in the size of PdO particle from 1 to 2 nm at 200 °C to 20 nm at 800 °C evidently occurred, while the particle size of the MgO support remained in the range of 50–100 nm, mainly because it had been pretreated at 900 °C.

Fig. 2 displays the H_2-TPR profiles of the PdO/MgO-T_1 samples. The PdO species in all samples were readily reduced to metallic Pd at 72 °C, but the reduction pattern appeared to be closely associated with the initial particle size. For example, the PdO/MgO-800 sample with larger PdO particles (ca. 20 nm) exhibits a negative reduction peak at 0 °C, corresponding to the decomposition of β-hydride palladium species, which are readily formed during hydrogen flushing at much lower temperatures [23]. Large Pd particles are capable of absorbing hydrogen within its structure to form a β-PdH_x and the amount of hydrogen involved in this process is usually dependent on the size of Pd particles [24]. The TPR patterns of other PdO/MgO-T_1 (T_1 < 800 °C) samples with smaller PdO particle sizes (1–10 nm) do not show any negative peak of hydrogen consumption, excluding the formation of palladium hydride species and confirming the direct reduction of PdO to Pd.

Upon further reduction of the PdO/MgO-T_1 samples with hydrogen, the resultant Pd/MgO catalysts exhibit variations in Pd particle size which strongly depends on the temperature of reduction. Fig. 3 shows the XRD patterns of the Pd/MgO catalysts. There is no Pd diffraction peak observed for the Pd/MgO-T_1–200 (T_1 = 200 and 400 °C) samples, indicating that the Pd particles are highly dispersed on the surfaces of MgO and therefore too small to be detected. On the other hand, Pd diffraction peaks are observed in the remaining Pd/MgO-T_1–T_2 samples. The average sizes of Pd

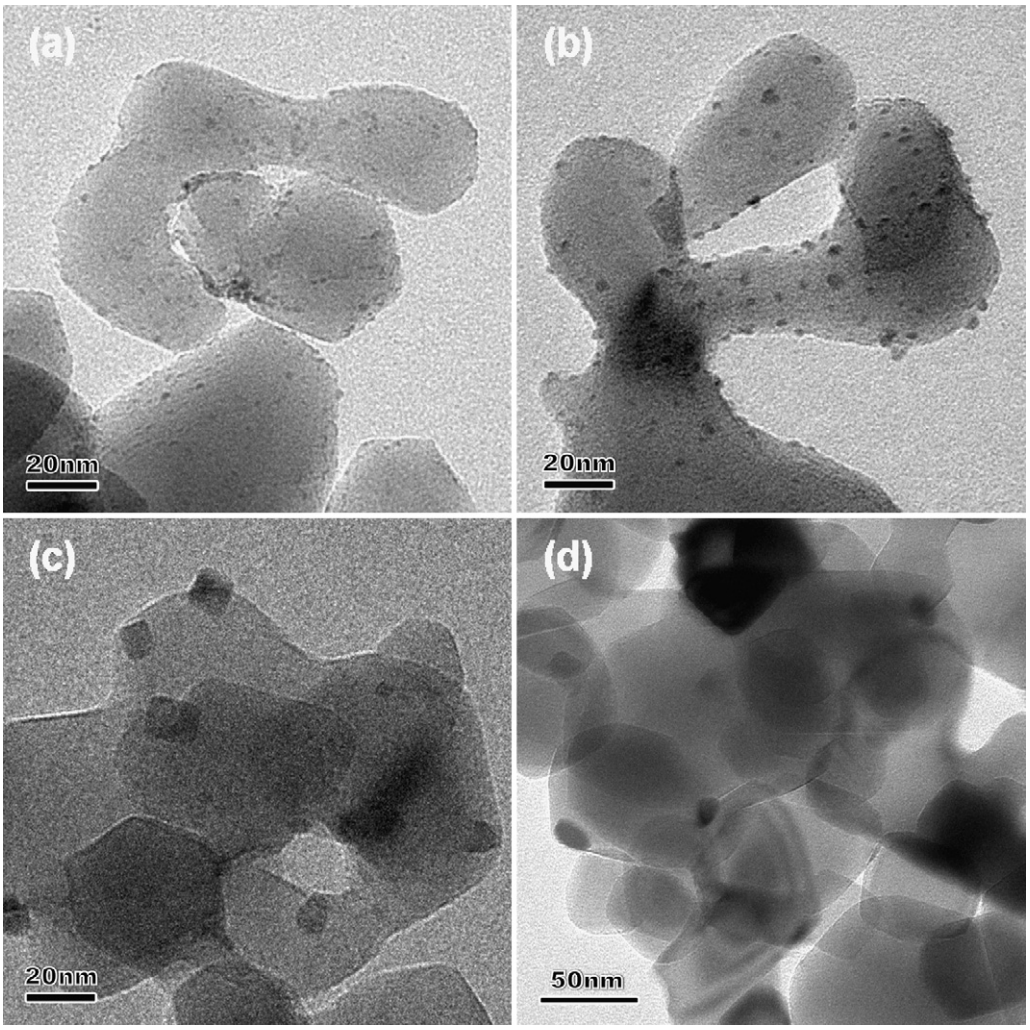

Fig. 1. TEM images of the PdO/MgO-T_1 precursors.

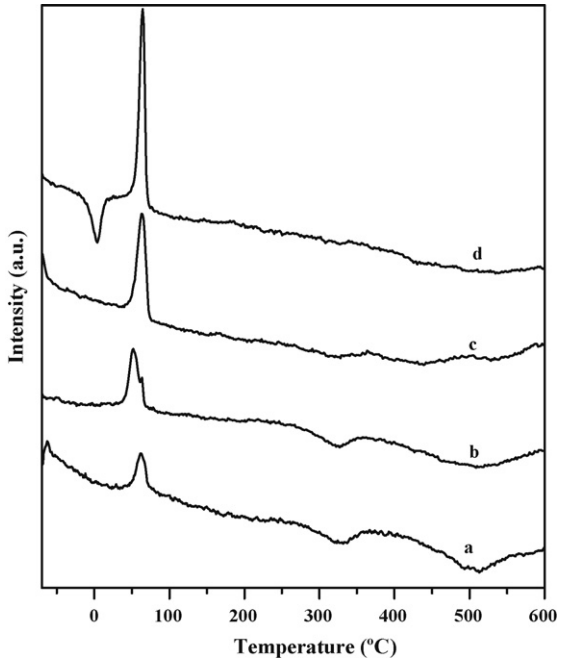

Fig. 2. H_2-TPR profiles of the PdO/MgO-T_1 precursors.

crystallites are in the range of 2–20 nm. Meanwhile, the diffraction peaks of MgO are observed in all the Pd/MgO samples, and the average crystalline size of MgO is 50–60 nm.

Fig. 4 shows the TEM images of the Pd/MgO catalysts and the estimated sizes of the Pd particles are summarized in Table 1. It is apparent that the Pd particles are predominately spherical in shape and are well dispersed on the surfaces of the MgO support. For the Pd/MgO-T_1–200 sample series, the sizes of Pd particles were dictated by the initial sizes of the PdO precursors, which increased from smaller than 2 nm in the Pd/MgO-200–200 sample up to 10 nm in the Pd/MgO-800–200 catalyst. On the other hand, the sizes of Pd particles in the Pd/MgO-800–T_2 series apparently increase with increasing temperature of reduction. Hydrogen reduction at 200 °C resulted in an average Pd particle size of 10 nm, whereas reduction treatment at 600 °C led to a drastic increase in Pd particle size to 20 nm. Meanwhile, the size and morphology of the MgO support remain practically unchanged in all the Pd/MgO catalysts. The MgO particles are mostly in flat shape and its average particle size ranges from 50 to 100 nm, in good agreement with the XRD results. Again, this might be due to the pre-treatment at 900 °C, which affords a rather stable MgO structure. That is, the subsequent calcination and reduction treatments, which were carried out at lower temperatures, had nearly no effect on the size and morphology of the MgO support.

Table 1 summarizes the average sizes of Pd particles in the Pd/MgO catalysts, estimated from the results of CO chemisorption.

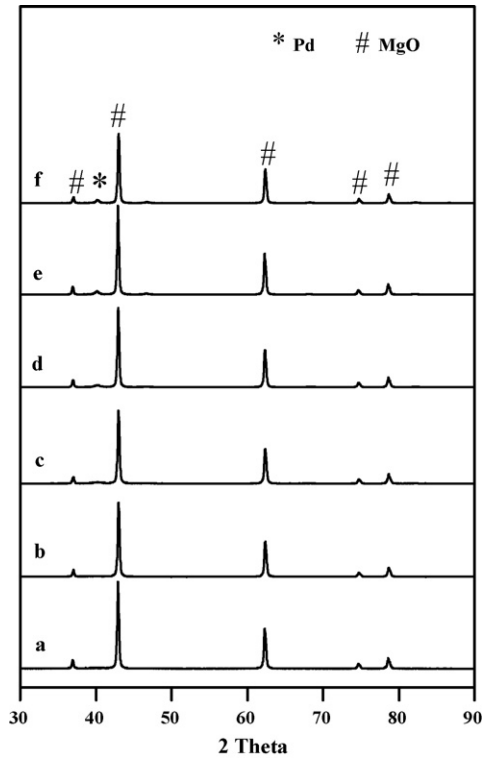

Fig. 3. XRD patterns of the Pd/MgO-T_1–T_2 catalysts.

The average size of Pd particle in the Pd/MgO-T_1–200 series increases from 1.8 to 11.9 nm with increasing calcination temperature (T_1) from 200 to 800 °C, corresponding to a decrease in Pd dispersion from 60% to 9%. For the Pd/MgO-800–T_2 series catalysts, an increase in the average Pd particle size with increasing hydrogen reduction temperature is observed, which varies from 11.9 nm at T_2 = 200 °C to 20.9 nm at T_2 = 600 °C. As a result, the Pd dispersion further decreases from 9% to 5%.

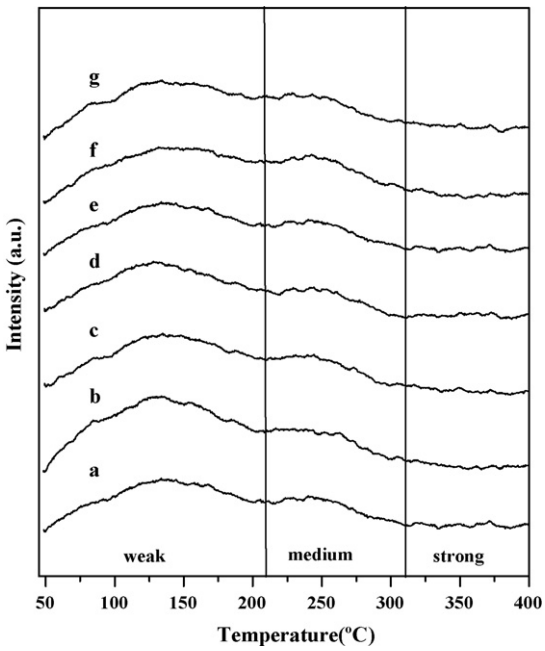

Fig. 5. Temperature programmed desorption (TPD) of CO_2 profiles of the bare MgO support and the Pd/MgO-T_1–T_2 catalysts.

Fig. 5 compares the CO_2-TPD profiles of the pure MgO support and the Pd/MgO catalysts. All samples show two main CO_2 desorption peaks, indicating the presence of basic sites with different strengths. Depending on the temperature of CO_2 desorption, the basic sites on the surface of MgO can be roughly catalogued into three regimes with weak (27–147 °C), medium (147–377 °C), and strong (above 377 °C) basicity [25,26]. The weak site should

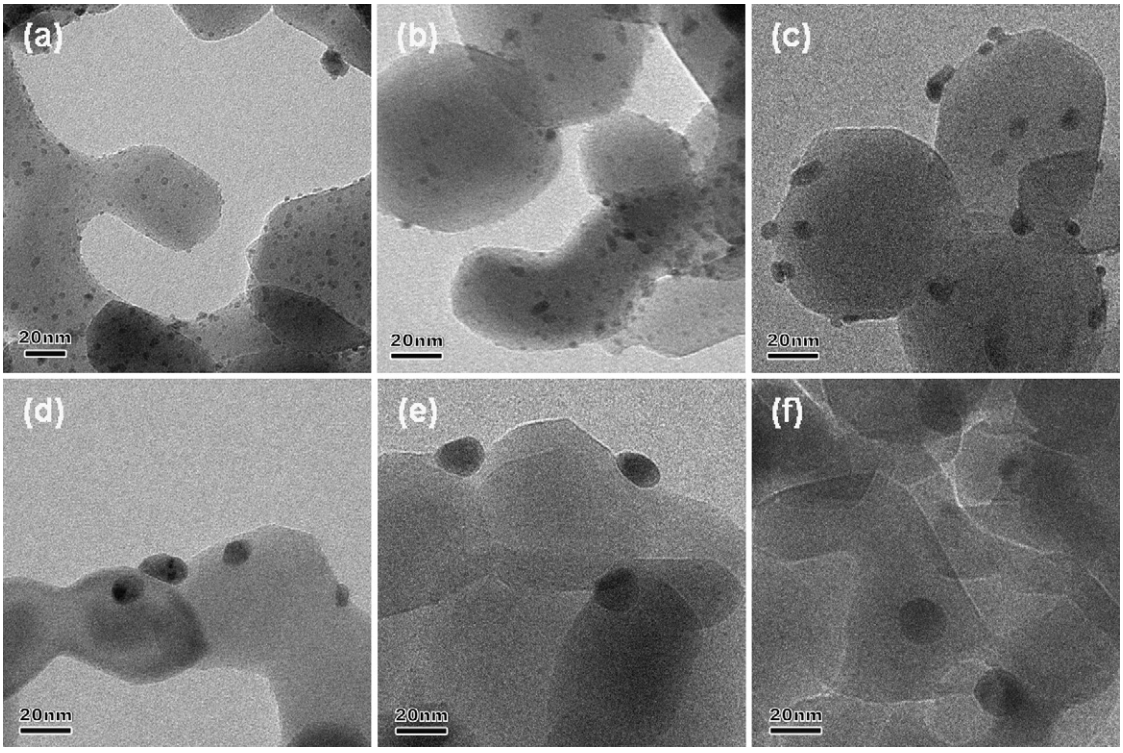

Fig. 4. TEM images of the Pd/MgO-T_1–T_2 catalysts.

Table 1
Physical and chemical properties of the Pd/MgO catalysts.

Catalyst	Pd surface area (m^2/g)	Pd dispersion (%)	Pd Particle size (nm)	
			d_1[a]	d_2[b]
Pd/MgO-200–200	5.3	59.7	1.8	1–2
Pd/MgO-400–200	4.6	51.8	2.2	~2
Pd/MgO-600–200	2.6	29.2	3.8	3–4
Pd/MgO-800–200	0.8	9.4	11.9	~10
Pd/MgO-800–400	0.6	6.8	16.6	10–20
Pd/MgO-800–600	0.5	5.4	20.9	15–25

[a] Measured by CO chemisorptions.
[b] Determined by TEM.

be associated with Brønsted basicity, mostly likely due to the lattice-bound OH groups. The medium and strong sites are probably associated with Lewis basicity arising from the three- and four-fold-coordinated O^{2-} anions [25]. Pure MgO support shows CO_2 desorptions at 130 and 250 °C, respectively, indicating the presence of weak and medium basic sites. The CO_2-TPD profiles of the PdO/MgO catalysts are in close resemblance to that of the bare MgO support, suggesting that their surface properties remain unchanged after the loading of Pd and the subsequent calcination and hydrogen reduction treatments.

3.2. Hydrogenation of isophorone and kinetic resolution of TMCH

Table 2 summarizes the reaction results of isophorone hydrogenation over the Pd/MgO catalysts. Obviously, the size of Pd particle strongly affects the conversion of isophorone, the chiral configuration, and the yield of TMCH. (*S*)-TMCH is produced when the Pd particle size is smaller than 4 nm. With increasing the size of Pd particle from 1.8 to 3.8 nm, the conversion of isophorone decreases from 100% to 80%, and the e.e. value of (*S*)-TMCH also decreases from 94% to 57%, but its yield increases from 21% to 47%. These small Pd nanoparticles are so active for the hydrogenation of isophorone that most of the isophorone are rapidly converted to racemic TMCH. The production of (*S*)-TMCH should result from the kinetic resolution of racemic TMCH, in which the (*R*)-TMCH enantiomer preferentially reacts with (*S*)-proline, leaving the (*S*)-TMCH enantiomer in excess [15,17]. The size of Pd particle significantly influences the rate of isophorone hydrogenation, but only slightly affects the following kinetic resolution of racemic TMCH. Thus, smaller Pd particles favor a higher isophorone conversion. These findings are consistent with the results of Török and co-workers [15].

As the size of Pd particle is larger than 10 nm, it is quite interesting that (*R*)-TMCH, rather than (*S*)-TMCH, is produced. This may be due to the considerable decrease in the hydrogenation activity of large Pd particle. The slow hydrogenation rate would provoke isophorone to condensate preferentially with (*S*)-proline to form proline–isophorone adducts, and the subsequent hydrogenation of the C=C bond of the intermediates would produce (*R*)-TMCH. As shown in Table 2, the e.e. value of (*R*)-TMCH decreases from 41% to 34% when the Pd particle size increases from 11.9 to 20.9 nm.

Table 2
Isophorone hydrogenation over the Pd/MgO catalysts.

Pd Particle size (nm)	e.e.%	Conversion%	Yield%
1.8	94 (*S*)	100	21
2.2	83 (*S*)	100	18
3.8	57 (*S*)	80	47
11.9	41 (*R*)	48	42
16.6	34 (*R*)	51	50
20.9	34 (*R*)	48	48

Reaction conditions: 32 mg catalyst, 110 mg (*S*)-proline, 1.18 mmol isophorone, 8.8 mL ethanol, 40 °C, H_2 3.0 MPa, 24 h.

Table 3
Kinetic resolution of racemic TMCH over the Pd/MgO catalysts.

Pd Particle size (nm)	e.e.%	Yield%	e.e.%[a]
1.8	71 (*S*)	25	94 (*S*)
2.2	87 (*S*)	27	83 (*S*)
3.8	98 (*S*)	47	57 (*S*)
11.9	30 (*S*)	84	41 (*R*)

Reaction conditions: 32 mg catalyst, 110 mg (*S*)-proline, 1.18 mmol TMCH, 8.8 mL ethanol, 40 °C, H_2 3.0 MPa, 24 h.
[a] e.e.% values for the hydrogenation of isophorone.

It seems that hydrogenation of the reaction intermediates also depends on the size of Pd particle.

Previous studies on enantioselective hydrogenation of isophorone over Pd catalysts [16,17,19,21] have confirmed that the secondary kinetic resolution of TMCH, generated by the direct hydrogenation of isophorone, is the key step for producing (*S*)-TMCH. Since (*R*)-TMCH was predominately produced with large Pd particles (>10 nm), the effect of Pd particle size on the kinetic resolution of racemic TMCH is further investigated. As shown in Table 3, the size of Pd particle does have a profound effect on the efficiency of kinetic resolution, but it does not reverse the chiral configuration of the product with the solely formation of (*S*)-TMCH. The catalyst with Pd particle size of 11.9 nm produces (*R*)-TMCH in the hydrogenation of isophorone, but (*S*)-TMCH in the kinetic resolution process. This fact excludes the possibility that excess of (*R*)-TMCH is produced by the kinetic resolution of TMCH. The catalyst with Pd particle size of 3.8 nm appears to be the most selective one in the kinetic resolution (e.e. ~98%), but its selectivity in the hydrogenation of isophorone is only 57%. These results further confirm that the process for producing excess of (*R*)-TMCH on large Pd particles is not the kinetic resolution.

To verify the origin of (*R*)-TMCH, the Pd/MgO catalyst with Pd particle size of 11.9 nm that gave R configuration was tested for hydrogenation of isophorone as a function of reaction time. As shown in Table 4, when the reaction was conducted from 12 to 24 h, the conversion of isophorone increased from 22% to 48% and the yield of (*R*)-TMCH increased from 13% to 42%. But the e.e. value of (*R*)-TMCH was only slightly varied, being 41–51%. This phenomenon can be ascribed not only to an increase in the conversion of isophorone with reaction time but also to the hydrogenation of C=C bond in the reaction intermediates. It can be proposed that isophorone initially condenses with proline to form a proline–isophorone adduct because of the slow hydrogenation rate

Table 4
Isophorone hydrogenation over the Pd/MgO catalyst with Pd particle size of 11.9 nm.

Reaction Time (h)	e.e.%	Conversion%	Yield%
12	51 (*R*)	22	13
24	41 (*R*)	48	42

Reaction conditions: 32 mg catalyst, 110 mg (*S*)-proline, 1.18 mmol isophorone, 8.8 mL ethanol, 40 °C, H_2 3.0 MPa.

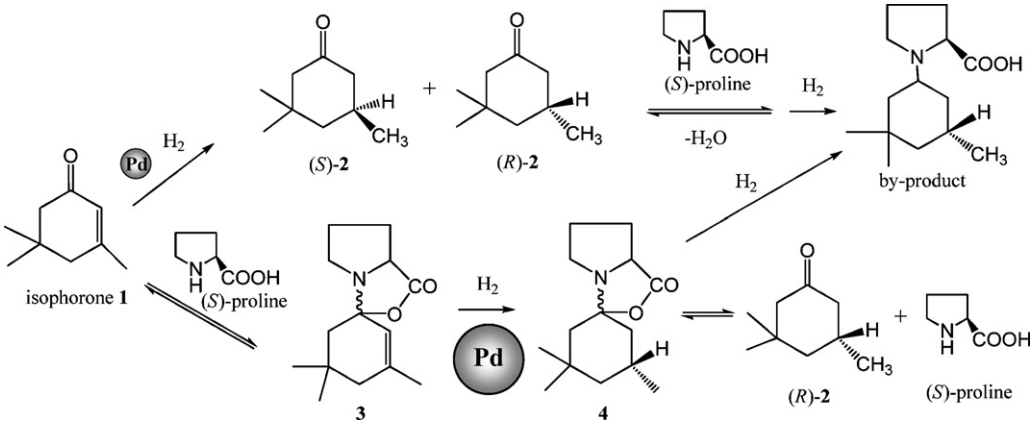

Scheme 1. Possible reaction pathways for the enantioselective hydrogenation of isophorone over the Pd/MgO catalysts in the presence of (*S*)-proline.

of isophorone over large Pd particles, and the subsequent hydrogenation of the C=C bond in the intermediate on Pd particles causes the formation of (*R*)-TMCH.

3.3. Reaction mechanism

As mentioned above, two possible mechanisms account for the enantioselective hydrogenation of isophorone over Pd catalysts, but the role of Pd particle is still under debate. The typical reaction pathway invokes the participation of Pd in the enantio-differentiating step, either through the initial condensation of (*S*)-proline with isophorone and the subsequent hydrogenation of the intermediate on Pd surface [6,7,11–14] or through the secondary kinetic resolution of racemic TMCH formed by the rapid hydrogenation of isophorone [15–17]. On the other hand, such a hypothesis is contradicted by several recent reports [18,19], which revealed that the enantioselectivity is merely the result of kinetic resolution that occurs homogeneously in the solution and that the Pd particles are not involved in the enantio-differentiating step. In this case, the Pd particles only serve to supply chemisorbed hydrogen required for hydrogenation of isophorone and are definitely not involved in the asymmetric induction. However, after a careful analysis of the reaction data supporting these mechanisms, it can be found that the size of Pd particle in the reported catalysts is mostly smaller than 10 nm and that (*S*)-TMCH is formed as the only chiral product.

As a matter of fact, (*R*)-TMCH was also formed in the enantioselective hydrogenation of isophorone on Pd catalysts, but the surface was modified by (−)-dihydroapovincaminic acid ethyl ester, (−)-DHVIN [26–29], instead of (*S*)-proline. Large Pd particles favorably give high e.e. value for this reaction, mainly because (−)-DHVIN is strongly adsorbed on large Pd particles and bonded with the substrate to form a reactant–modifier complex, and the following hydrogenation of the intermediate complex gives (*R*)-TMCH [26]. It is most likely that the large Pd particles have the ability to accommodate the substrate–modifier adduct in an appropriate conformation on their surfaces where the enantio-differentiation takes place smoothly for the production of (*R*)-TMCH. In our case, when the Pd particle size is larger than 10 nm, the hydrogenation of isophorone in the presence of (*S*)-proline may be similar to that described in (−)-DHVIN modified Pd catalysts.

Therefore, we propose a competitive reaction network to clarify the origin of (*R*)-TMCH obtained on larger Pd particles. As illustrated in Scheme 1, well-dispersed Pd particle (<4 nm) favors a rapid hydrogenation of isophorone that primarily yields racemic TMCH (R-**2** and S-**2**), and then, the subsequent kinetic resolution of racemic TMCH results in (*S*)-TMCH. This is consistent with the commonly reported reaction mechanism in which Pd particles participate in the enantioselective reaction [15–17]. On the other hand, over the Pd/MgO catalysts with Pd particle size exceeding 10 nm, mainly because of the slow hydrogenation rate, isophorone preferentially undergoes condensation with (*S*)-proline to form an oxazolidone type intermediate **3**, which is commonly regarded as the most probable reaction intermediate [12,30]. Hydrogenation of this intermediate on the Pd particle generates the enantioselectivity in compound **4**. Further hydrolysis of compound **4** gives (*R*)-TMCH, whereas its hydrogenation leads to the formation of fully hydrogenated compounds which significantly influence the yield of TMCH. Hence, the reaction route of enantioselective hydrogenation of isophorone is closely related to the properties of the Pd/MgO catalysts, especially the size of Pd particles that determines the configuration of the product.

4. Conclusions

The heterogeneous enantioselective hydrogenation of isophorone in the presence of (*S*)-proline over Pd/MgO catalysts is systematically studied with varying Pd particle size, which determines the configuration of the chiral product. For the first time, (*R*)-TMCH was obtained in the presence of (*S*)-proline over Pd/MgO catalysts with Pd particle size exceeding 10 nm. It is concluded that the Pd metal surfaces not only serve to supply chemisorbed hydrogen for hydrogenation of isophorone but also involve in the enantio-differentiating step. Two competitive reactions occurring in the hydrogenation of isophorone were identified; namely the enantioselective hydrogenation of reaction intermediates formed between isophorone and (*S*)-proline on larger Pd particles (>10 nm) leads to the formation of excess (*R*)-TMCH enantiomer, while the primary hydrogenation of isophorone yields racemic TMCH over Pd particles smaller than 4 nm, followed by kinetic resolution leaving the (*S*)-TMCH enantiomer in excess. These results shed some new lights on the mechanism of enantioselective hydrogenation of isophorone, which has been a subject of actively debated in the past decade.

Acknowledgments

The financial supports of this work from the National Natural Science Foundation of China (Grant No. 20621063) and National Science Council, Taiwan (NSC95-2113-M-001-040-NY3) are gratefully acknowledged.

References

[1] Y. Orito, S. Imai, S. Niwa, J. Chem. Soc. Jpn. (1979) 1118.
[2] Y. Izumi, M. Imaida, H. Fukawa, S. Akabori, Bull. Chem. Soc. Jpn. 36 (1963) 21.
[3] T. Mallat, E. Orglmeister, A. Baiker, Chem. Rev. 107 (2007) 4863.

[4] T. Burgi, A. Baiker, Acc. Chem. Res. 37 (2004) 909.
[5] M. Studer, H.U. Blaser, C. Exner, Adv. Synth. Catal. 345 (2003) 45.
[6] A. Tungler, React. Kinet. Catal. Lett. 74 (2001) 271.
[7] A. Tungler, E. Sipos, V. Hada, Curr. Org. Chem. 10 (2006) 1569.
[8] Y. Nitta, J. Synth. Org. Chem. Jpn. 64 (2006) 827.
[9] E. Klabunovskii, G.V. Smith, Á. Zsigmond, in: B. James, P.W.N.M.V. Leeuwen (Eds.), Heterogeneous Enantioselective Hydrogenation: Theory and Practice Series: Catalysis by Metal Complexes, Springer, The Netherlands, 2006.
[10] A. Tungler, M. Kajtar, T. Mathe, G. Toth, E. Fogassy, J. Petro, Catal. Today 5 (1989) 159.
[11] A. Tungler, T. Mathe, J. Petro, T. Tarnai, J. Mol. Catal. 61 (1990) 259.
[12] M. Fodor, A. Tungler, L. Vida, Catal. Today 140 (2008) 58.
[13] E. Sipos, A. Tungler, I. Bitter, J. Mol. Catal. A: Chem. 198 (2003) 167.
[14] E. Sipos, A. Tungler, G. Fogassy, J. Mol. Catal. A: Chem. 216 (2004) 171.
[15] S.C. Mhadgut, I. Bucsi, M. Török, B. Török, Chem. Commun. (2004) 984.
[16] S.C. Mhadgut, M. Török, J. Esquibel, B. Török, J. Catal. 238 (2006) 441.
[17] S.C. Mhadgut, M. Török, S. Dasgupta, B. Török, Catal. Lett. 123 (2008) 156.
[18] A.I. McIntosh, D.J. Watson, J.W. Burton, R.M. Lambert, J. Am. Chem. Soc. 128 (2006) 7329.
[19] A.I. McIntosh, D.J. Watson, R.M. Lambert, Langmuir 23 (2007) 6113.
[20] E.S. Zhan, S. Li, Y.D. Xu, W.J. Shen, Catal. Commun. 8 (2007) 1239.
[21] S. Li, E.S. Zhan, Y. Li, Y.D. Xu, W.J. Shen, Catal. Today 131 (2008) 347.
[22] H.P. Klug, L.E. Alexander, X-Ray Diffraction Procedures: For Polycrystalline and Amorphous Materials, 2nd ed., Wiley, New York, 1974.
[23] M. Boudart, H.S. Hwang, J. Catal. 39 (1975) 44.
[24] C. Amorim, M.A. Keane, J. Colloid Interface Sci. 322 (2008) 196.
[25] Z. Liu, J.A. Cortés-concepción, M. Mustian, M.D. Amiridis, Appl. Catal. A: Gen. 302 (2006) 232.
[26] T. Tarnai, A. Tungler, T. Mathe, J. Petro, R.A. Sheldon, G. Toth, J. Mol. Catal. A: Chem. 102 (1995) 41.
[27] A. Tungler, T. Mathe, T. Tarnai, K. Fodor, G. Toth, J. Kajtar, I. Kolossvary, B. Herenyi, R.A. Sheldon, Tetrahedron: Asymmetry 6 (1995) 2395.
[28] G. Farkas, L. Hegedus, A. Tungler, T. Mathe, J.L. Figueiredo, M. Freitas, J. Mol. Catal. A: Chem. 153 (2000) 215.
[29] G. Farkas, E. Sipos, A. Tungler, A. Sarkany, J.L. Figueiredo, J. Mol. Catal. A: Chem. 170 (2001) 101.
[30] D. Seebach, A.K. Beck, D.M. Badine, M. Limbach, A. Eschenmoser, A.M. Treasurywala, R. Hobi, W. Prikoszovich, B. Linder, Helv. Chim. Acta 90 (2007) 425.